Cloud-Base Height Estimation from VIIRS. Part I: Operational Algorithm Validation against *CloudSat*

CURTIS J. SEAMAN, YOO-JEONG NOH, AND STEVEN D. MILLER

Cooperative Institute for Research in the Atmosphere, Colorado State University, Fort Collins, Colorado

ANDREW K. HEIDINGER

NOAA/NESDIS/Center for Satellite Applications and Research/Advanced Satellite Products Branch, Madison, Wisconsin

DANIEL T. LINDSEY

NOAA/NESDIS/Center for Satellite Applications and Research/Regional and Mesoscale Meteorology Branch, Fort Collins, Colorado

ABSTRACT

The operational VIIRS cloud-base height (CBH) product from the *Suomi–National Polar-Orbiting Partnership* (*SNPP*) satellite is compared against observations of CBH from the cloud profiling radar (CPR) on board *CloudSat*. Because of the orbits of *SNPP* and *CloudSat*, these instruments provide nearly simultaneous observations of the same locations on Earth for a ~4.5-h period every 2–3 days. The methodology by which VIIRS and *CloudSat* observations are spatially and temporally matched is outlined. Based on four 1-month evaluation periods representing each season from June 2014 to April 2015, statistics related to the VIIRS CBH retrieval performance have been collected. Results indicate that when compared against *CloudSat*, the VIIRS CBH retrieval does not meet the error specifications set by the Joint Polar Satellite System (JPSS) program, with a root-mean-square error (RMSE) of 3.7 km for all clouds globally. More than half of all matching VIIRS pixels and *CloudSat* profiles have CBH errors exceeding the 2-km error requirement. Underscoring the significance of these statistics, it is shown that a simple estimate based on a constant cloud geometric thickness of 2 km outperforms the current operational CBH algorithm. It was found that the performance of the CBH product is impacted by the accuracy of upstream retrievals [primarily cloud-top height (CTH)] and the a priori information used by the CBH retrieval algorithm. However, even when CTH errors were small, CBH errors still exceed the JPSS program error specifications with an RMSE of 2.3 km.

1. Introduction

Cloud-base height (CBH) is an important parameter for numerous applications—perhaps most notably for aviation, as fog and low ceilings pose flight hazards in terms of reduced surface visibility (Gultepe et al. 2009; Leyton and Fritsch 2004; Herzegh et al. 2015; Inoue et al. 2015). CBH is a necessary component of cloud-free line of sight (CFLOS) calculations, which have numerous aviation and military applications (Reinke and Vonder Haar 2011). CBH and the related parameters of cloud-base temperature and cloud-base pressure directly impact downwelling longwave radiative fluxes, which feed back to global radiative balance and climate (Slingo and Slingo 1988; Baker 1997). CBH is an important parameter in the hydrologic cycle, as it may be a determining factor as to whether falling hydrometeors will reach the surface as precipitation or evaporate as virga. CBH has been shown to govern cloud microphysics (Johnson 1980), and it may be related to convective storm strength and lightning activity (Fuchs et al. 2015).

Given this importance, the aviation community and other users [e.g., the National Weather Service (NWS) Operational Advisory Team (NOAT)] have issued a requirement for global retrievals of CBH from satellite

---

ⓐ Denotes content that is immediately available upon publication as open access.

Corresponding author e-mail: Curtis J. Seaman, curtis.seaman@colostate.edu

platforms. A variety of methods for retrieving CBH using different satellite instruments have been developed. These include passive microwave (Pandey et al. 1983), combined infrared (IR) and microwave (Wilheit and Hutchison 1997), remote sensing in the oxygen A band (Kokhanovsky and Rozanov 2005), and a spectral radiance matching algorithm that combines radar and lidar observations with visible and IR imagery (Sun et al. 2016). Algorithms for retrieving or estimating cloud-base height from passive visible and IR imagery have been developed by Minnis et al. (1997), Bendix et al. (2005), Hutchison (2002), and Hutchison et al. (2006). In addition, there have been several data fusion methods to blend visible and IR satellite imagery with ground-based observations (e.g., Forsythe et al. 2000; Ellrod 2002; Herzegh et al. 2015; Calvert et al. 2016) to create a CBH analysis product. Bankert et al. (2004) developed a data mining algorithm that relates visible and IR satellite imagery with numerical weather prediction (NWP) model output for the purpose of determining cloud ceilings.

The Joint Polar Satellite System (JPSS) program, a collaborative effort between the U.S. agencies of National Oceanic and Atmospheric Administration (NOAA) and National Aeronautics and Space Administration (NASA) for the next generation of polar-orbiting environmental satellites (Goldberg et al. 2013), selected the retrieval algorithm of Hutchison (2002) and Hutchison et al. (2006) as one of ~30 environmental data records (EDRs) to be produced operationally through the interface data processing segment (IDPS). With the launch of the Visible Infrared Imaging Radiometer Suite (VIIRS) on board the *Suomi–National Polar-Orbiting Partnership* (*SNPP*) satellite (a ''risk reduction'' satellite to the operational JPSS series) in late 2011 (Hillger et al. 2013), the Hutchison CBH retrieval algorithm (hereinafter IDPS retrieval algorithm) became the first global retrieval of CBH from passive visible and IR satellite data to be produced operationally. The IDPS retrieval algorithm is designed to retrieve CBH for any and all clouds, in contrast to the fog and low stratus (FLS) product (Calvert et al. 2016), which is specific to near-surface cloud cover and is currently planned for operational distribution by the GOES-R program (Schmit et al. 2005).

In this work, the performance of the IDPS retrieval is evaluated by comparing against direct observations of CBH from *CloudSat* (Stephens et al. 2002). The primary instrument on board *CloudSat* is a cloud profiling radar (CPR) capable of resolving the geometric profile of clouds at a vertical resolution of 240 m. *CloudSat* and *SNPP* are located in the same orbital plane, albeit at different altitudes, providing routine ''matchup periods,'' where the CBH retrievals from *CloudSat* and VIIRS are collocated in space and time. These matchup periods provide a large sample size and robust statistics of the performance of the IDPS algorithm globally as compared with the relatively small number and sparse distribution of instrumented ground-based sites where CBH is routinely observed (Fitch et al. 2016). The IDPS algorithm is evaluated as a function of cloud optical thickness and cloud phase classification for monthlong periods in each of the four seasons spanning the period June 2014–April 2015.

While the IDPS CBH retrieval algorithm does not change between day and night, this work is limited to the evaluation of daytime retrievals. This limitation is due to battery issues on board *CloudSat* that preclude the operation of the CPR at night since April 2011 (Nayak et al. 2012). As discussed in the next section, the IDPS algorithm relies on upstream retrievals of cloud optical thickness (COT) τ and effective particle size (EPS), and these quantities are difficult to retrieve at night (Walther et al. 2013). Therefore, it is very likely that the nighttime CBH retrieval performance would be degraded relative to the results shown here for daytime-only retrievals.

The Cloud–Aerosol Lidar with Orthogonal Polarization (CALIOP) on board the *Cloud–Aerosol Lidar and Infrared Pathfinder Satellite Observations* (*CALIPSO*) satellite (Winker et al. 2009) is another active sensor capable of profiling clouds and, as with *CloudSat*, provides similar routine matchup periods where the lidar retrievals are collocated in space and time with VIIRS. However, signal attenuation of the CALIOP lidar is total for clouds with optical thickness > ~3. This precludes the validation of CBH for clouds with greater optical thickness. While observations of cloud-top height (CTH) from *CloudSat* are compared against the operational IDPS CTH product in this study, it is noted that the lidar on board *CALIPSO* is better suited to evaluate the IDPS CTH retrieval product (Heidinger et al. 2010a,b). CTH comparisons between *CloudSat* and VIIRS are included here only to determine which errors in CBH are due to the IDPS CBH retrieval itself and which are due to errors in upstream IDPS products.

This paper is outlined as follows: Section 2 describes the IDPS CBH retrieval algorithm. Section 3 describes the *CloudSat* instrument, which is used to validate the IDPS CBH retrieval and the collocation of the *CloudSat* profiles with VIIRS pixels for the development of the ''matchup'' dataset used in this work. Section 4 presents the results and analysis of the performance of the IDPS CBH retrieval. Conclusions and additional discussion on the retrieval of CBH from passive IR sensors are found in section 5.

2. The VIIRS IDPS cloud base height retrieval algorithm

The operational VIIRS CBH retrieval produced by the IDPS (Baker 2011) is based on the algorithm developed

TABLE 1. VIIRS IDPS cloud classification ([Baker 2011](#)). CTH, EPS, and τ are used to define cloud type. For liquid and mixed-phase clouds, EPS = r_e. For ice clouds, EPS = D_e. LWC is a predefined average LWC used in the CBH retrieval [Eq. (2)].

Cloud type	CTH (km)	EPS (μm)	τ	LWC (g m^{-3})
Altocumulus/altostratus	1.5–5.5	4–30	2–32	0.455
Cirrus	6–12	10–100	0.01–5	0.01
Cirrocumulus	6–15	30–120	1–8	0.01
Cumulus	0.2–6.5	5–50	3–50	0.580
Cumulonimbus/nimbostratus	0.2–6.5	10–100	3–50	0.01
Stratus	0–2.5	2–25	1–10	0.293

by [Hutchison (2002)](#) and [Hutchison et al. (2006)](#). This algorithm, referred to as the IDPS retrieval algorithm in this study, is briefly described here. This algorithm retrieves cloud geometric thickness (CGT) and subtracts this value from an upstream retrieval of CTH to determine CBH; that is,

$$CBH = CTH - CGT. \tag{1}$$

The retrieval of CGT varies depending on whether the cloud is assumed to be primarily composed of liquid droplets or ice particles and is dependent on an upstream retrieval of cloud phase. The cloud phase algorithm is described in the algorithm theoretical basis document (ATBD) for the VIIRS cloud mask ([Baker 2014](#)). For liquid clouds, CGT is defined as the ratio between the liquid water path (LWP) and the cloud-averaged liquid water content (LWC):

$$CGT_{liq} = \frac{LWP}{LWC}. \tag{2}$$

It can be shown (e.g., [Stephens 1994](#)) that the LWP is related at first order (under the assumption of a vertically homogeneous cloud profile) to τ, cloud droplet effective radius r_e, and the density of liquid water ρ_{liq} as follows:

$$LWP = \frac{2}{3} \rho_{liq} \tau r_e. \tag{3}$$

The CBH algorithm makes use of upstream retrievals of optical thickness and effective radius and assumes $\rho_{liq} = 1 \, g \, cm^{-3}$. Values of LWC used in Eq. (2) are predefined for each cloud type (specified in Table 1) and are assumed constant. In addition to the upstream cloud type retrieval outlined in Table 1, an upstream cloud phase retrieval is also used as input to the CBH algorithm. The five cloud phase classifications include water, cirrus, opaque ice, mixed phase, and overlap. Only those clouds classified as water use the CGT defined by Eq. (2). All other clouds use the ice-phase CGT defined below.

For ice-phase clouds, CGT is the ratio of the ice water path (IWP) and ice water content (IWC):

$$CGT_{ice} = \frac{IWP}{IWC}, \tag{4}$$

where IWP is related to COT and ice particle effective diameter D_e based on the regression of [Liou (1992)](#):

$$IWP = \frac{\tau}{a + \dfrac{b}{D_e}}, \tag{5}$$

where $a = -0.006\,656$ and $b = 3.686$. This regression is based on a model of the radiative properties of hexagonal ice crystals using representative ice particle size distributions found in cirrus clouds and has a stated accuracy of 1% ([Liou 1992](#)).

In contrast to liquid-phase clouds, where LWC is held fixed, the IWC used in Eq. (4) varies as a function of temperature. For a cloud layer with a mean temperature T_m (K; [Hutchison et al. 2006](#)),

$$IWC = \exp\{-7.6 + 4\exp[-2.443\times10^{-4}(253 - T_m)^{2.445}]\}, \tag{6}$$

where IWC has units of g m^{-3}. The mean temperature T_m is related to cloud-top temperature T_{ct} and optical thickness as follows:

$$T_m = MIN\left\{\left[MAX(213, T_{ct}) + \frac{20}{6}\tau\right], 253\right\}, \tag{7}$$

where T_m is allowed to vary only between 213 and 253 K. The optical thickness premultiplier constant in Eq. (7) represents the gradient of cloud-top temperature with respect to optical thickness.

For clouds with a retrieved mean temperature less than 218 K, the retrieved IWC value from Eq. (6) is less than 1.3×10^{-3} g m^{-3}. While it is difficult to accurately measure IWC, values less than 1×10^{-3} g m^{-3} are likely at or below the detection limit of common microphysical probes used to measure IWC on aircraft (see, e.g., [Lawson and Baker 2006](#)). Furthermore, such small values of IWC, when used in Eq. (4), lead to excessively large CGT values with errors of up to an order of magnitude or more. This issue primarily impacts

optically thin clouds, as the mean temperature retrieved from Eq. (6) can be only less than 218 K if the optical depth is less than 1.5. Limiting T_{ct} to 213 K or warmer in Eq. (6) was intended to mitigate this issue. As will be demonstrated in section 4, this often results in the retrieval of "cirrus" cloud-base heights within the boundary layer. While the ATBD adopted by the JPSS program (Baker 2011) recommended capping cirrus CGT values at 3 km to resolve this issue, results shown in section 4 indicate this adjustment was never implemented operationally.

It should be noted that while VIIRS is sensitive to total cloud optical thickness within the line of sight of the instrument, the upstream algorithms utilized by the CBH retrieval do not discriminate the optical thickness contributions from multiple cloud layers. The COT and EPS retrievals were developed and evaluated assuming a single-layer cloud exists (Ou et al. 2003). Furthermore, optically thick mid- and upper-level clouds may obscure lower-level clouds. As a result, the CGT retrieval described above is only applicable to a single-layer cloud and because the CTH retrieval applies to the top of the uppermost cloud layer, the retrieved CBH is assumed to apply to the base of the uppermost cloud layer. The performance of the CBH retrieval is expected to be poor in cases containing multiple cloud layers, as the total COT is attributed to the uppermost cloud layer. Overlapping cloud layers are detected using the algorithm of Ou et al. (1998).

The JPSS program has defined a set of performance requirements for the IDPS CBH retrieval (Baker 2011). Of primary concern for this study is the specified measurement uncertainty of 2 km. From the perspective of the aviation community, this is not a stringent requirement. While a retrieval error of 2 km meets this specification, it is far greater than the errors in ceilometer measurements of CBH, which are typically less than 100 m (e.g., Eberhard 1986). However, ceilometer measurements are point observations whose applicability to the regional cloud field is a strong function of cloud type and airmass properties (e.g., Forsythe et al. 2000; Miller et al. 2014). Satellite-based estimation techniques extend these estimates globally.

We note here that there are two versions of the operational IDPS CBH product: the intermediate product (IP) and the EDR. The IP maintains the native resolution of the VIIRS instrument (~750 m at nadir), while the EDR aggregates the VIIRS pixels to a 6 km-resolution grid. The results presented in section 4 use the IP, which better matches the CloudSat footprint and conducts no averaging to the pixel-level upstream products that feed into the CBH estimates.

The IDPS is responsible for producing τ, EPS (either liquid r_e or D_e), CTH, T_{ct}, cloud phase, and cloud type classification retrievals that are required as input into the CBH retrieval. These retrievals are contained in the cloud optical properties (COP), CTH, and cloud cover and layers (CCL) IPs and EDRs. Descriptions of these algorithms are available in the ATBDs and operational algorithm description (OAD) documents, which are made available online by the JPSS program (http://npp.gsfc.nasa.gov/documents.html; http://www.star.nesdis.noaa.gov/jpss/Docs.php).

Figure 1 shows the flowchart of the IDPS processing chain that retrieves CBH from the VIIRS sensor data records (SDRs; calibrated visible reflectance and IR brightness temperature data). Cao et al. (2013a) describe the calibration of VIIRS SDRs. A parallax correction is applied to the CTH and COP retrievals to account for the fact that, at off-nadir satellite viewing angles, the observed cloud-top properties are geolocated (i.e., projected along the instrument's line of sight to the reference ellipsoid) to a different latitude and longitude than the subcloud-base location. The parallax correction shifts the horizontal location of the cloud and its retrieved properties toward the satellite subpoint to correct for this displacement error. The parallax correction also flags pixels that are obscured from view due to optically thick high clouds along the satellite line of sight. The CGT retrieval assumes the input cloud properties to be valid for a vertical cloud thickness, rather than the slant path viewed by the VIIRS instrument for off-nadir pixels (Hutchison 2002; Hutchison et al. 2006). The parallax correction algorithm is discussed in the VIIRS perform parallax correction (PPC) OAD (Baker 2013; also available at http://npp.gsfc.nasa.gov/documents.html). As CBH is the final step of a long processing chain, errors in upstream retrievals and errors in LWC and IWC accumulate as errors in CGT, which translate directly to errors in CBH.

3. Matching *CloudSat* and VIIRS

In this paper, we evaluate the performance of the VIIRS IDPS CBH retrieval by comparing the VIIRS retrievals against observations from the *CloudSat* CPR. In this section, we describe the *CloudSat* CPR, define matchup periods where *CloudSat* and *SNPP* VIIRS observations are nearly collocated in space and time, and describe the methodology by which VIIRS CBH retrievals are extracted and compared against *CloudSat* observations.

The *CloudSat* CPR is a near-nadir-pointing (0.16° forward), nonscanning W-band (94 GHz; 3 mm) cloud radar with a field of view of ~1.3 km in the across-track dimension and ~1.7 km in the along-track dimension.
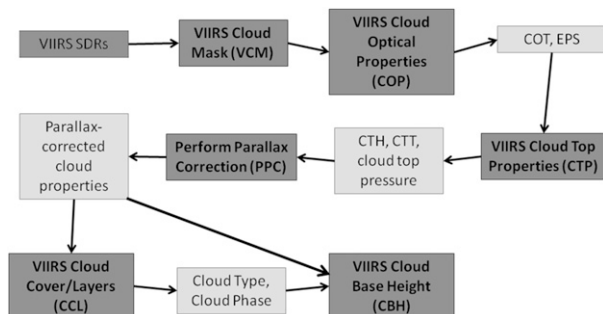
FIG. 1. The IDPS algorithm processing chain for the retrieval of CBH. COT is cloud optical thickness (τ); EPS is effective particle size (r_e for liquid clouds, D_e for ice clouds); CTT is cloud top temperature. Dark shaded boxes are operational products that are independently validated by the JPSS program. Lighter shaded boxes indicate inputs to downstream products that are used by the CBH product.

Profiles are collected every 1.1 km, which leads to oversampling along the ground track. While the vertical resolution of the CPR range gates is 480 m, oversampling increases the effective vertical resolution to ∼240 m. Additional details of the *CloudSat* CPR are found in Stephens et al. (2002, 2008) and Tanelli et al. (2008).

In this study, the *CloudSat* geometric profile product (2B-GEOPROF) and the *CloudSat* 2C precipitation column algorithm (2C-PRECIP-COLUMN) operational data products (available at http://www.cloudsat.cira.colostate.edu/data-products/level-2b) were utilized. The 2B-GEOPROF product contains the calibrated radar reflectivity and the CPR cloud mask. The CPR cloud mask is used to identify CTH and CBH in the *CloudSat* observations, while the radar reflectivity is used as a sanity check against those estimates. The 2B-GEOPROF product is described in Marchand et al. (2008). CBH is difficult to define in precipitating clouds. Also, the *CloudSat* CPR is sensitive to light rain, which attenuates the signal. Thus, *CloudSat* profiles likely containing precipitation were excluded from this analysis. Precipitation is identified using the path-integrated attenuation algorithm of Haynes et al. (2009), which is included in the 2C-PRECIP-COLUMN product.

For a CPR profile containing a single-layer cloud, CBH is defined as the height above mean sea level (MSL) of the lowest range gate in the profile that is identified as cloudy according to the CPR cloud mask. In cases where multiple cloud layers exist in a CPR profile, CBH is defined as the base of the uppermost cloud layer. This was done for consistency with the IDPS algorithm, as VIIRS is only capable of retrieving CBH for the uppermost cloud layer. CTH is defined as the height above MSL of the highest range gate identified as cloudy in the CPR cloud mask, except that clouds with CTH

exceeding 20 km MSL were excluded. The IDPS CBH retrieval is valid only for clouds between 0 and 20 km MSL (Baker 2011).

A battery anomaly on board the *CloudSat* satellite in April 2011 (prior to the launch of *SNPP*) has limited operation of the CPR to the daytime side of Earth (Nayak et al. 2012). While *CloudSat* is part of the A-Train satellite constellation (Stephens et al. 2002), this battery anomaly made it difficult to maintain tight formation flying and *CloudSat* has since been relocated a safe distance away from the rest of the A-Train but within the same orbit. As a result, the 2B-GEOPROF-LIDAR product is no longer available. The 2B-GEOPROF-LIDAR product combines information from the CPR cloud mask with lidar observations from the CALIOP on board the *CALIPSO* satellite (Winker et al. 2009) to improve detection of optically thin clouds often missed by the *CloudSat* CPR (Mace and Zhang 2014).

Another limitation of the *CloudSat* CPR is the presence of ground clutter. Ground clutter is caused by sidelobes of the radar pulse that reflect off the surface and create a distribution of anomalous returns. These artifacts impact the first three range gates above the surface (impacting the layer from the surface to ∼750 m) and limit the ability of *CloudSat* to detect clouds within this layer (Marchand et al. 2008). To ensure that cloud detection is not impacted by ground clutter, *CloudSat* profiles where the observed CBH and/or CTH are less than 1 km above ground level (AGL) were excluded. Furthermore, VIIRS retrievals of CTH and/or CBH below 1 km AGL were similarly excluded from consideration, as *CloudSat* is unable to validate these retrievals. The *CloudSat* digital elevation map (DEM), contained within the 2B-GEOPROF product, was used to determine height AGL.

As mentioned above, the IDPS CBH IP evaluated here maintains the native resolution of the VIIRS instrument, which is ∼750 m at nadir and decreases to ∼1.5 km at the scan edge (Cao et al. 2013b). The higher spatial resolution of VIIRS compared to the *CloudSat* CPR results in as many as 12 VIIRS pixels that at least partially overlap a single *CloudSat* profile (at VIIRS nadir) and as few as two (at the edge of scan). For this work, we selected the VIIRS CBH retrieval for the overlapping pixel that is closest to the center of the *CloudSat* profile that does not contain any error fill values. Error fill values are provided for the following circumstances: clouds are not detected in the pixel [error (ERR)], the parallax-corrected CTH indicated that opaque high clouds obscure the view of adjacent pixels with lower CTH [not available (N/A)], a required input from an upstream retrieval was missing [value does not exist (VDNE)]; the retrieved CBH or CTH was outside

TABLE 2. Summary of *CloudSat*–VIIRS matchup periods. See text for definitions on exclusions, Within CTH Spec and Within CBH Spec. "*CloudSat* only" refers to *CloudSat* detecting cloud when VIIRS did not. "VIIRS only" refers to VIIRS detecting cloud when *CloudSat* did not. Unless otherwise specified, percentages provided in bold are relative to the total number of matchup points and are rounded to the nearest tenth. Note: matchup points may be excluded for more than one reason. As a result, the sum of all percentages of excluded points may exceed 100%.

Month	June 2014	September 2014	January 2015	April 2015
Matchup periods	12	11	12	12
Matchup points	662 343	540 023	560 917	588 604
Excluded points				
ERR	210 451 **(31.8%)**	158 299 **(29.3%)**	194 626 **(34.7%)**	206 350 **(35.1%)**
N/A	6071 **(0.9%)**	4793 **(0.9%)**	4877 **(0.9%)**	5179 **(0.9%)**
OGPT/OBPT	16 018 **(2.4%)**	10 715 **(2.0%)**	10 922 **(1.9%)**	15 322 **(2.6%)**
VDNE	126 **(0.0%)**	40 **(0.0%)**	0 **(0.0%)**	950 **(0.2%)**
OOR	15 **(0.0%)**	232 **(0.0%)**	62 **(0.0%)**	142 **(0.0%)**
Precipitation	45 053 **(6.8%)**	42 589 **(7.9%)**	50 075 **(8.9%)**	53 272 **(9.1%)**
Ground clutter	194 036 **(29.3%)**	164 624 **(30.5%)**	171 069 **(30.5%)**	171 790 **(29.2%)**
CloudSat only	30 507 **(4.6%)**	30 973 **(5.7%)**	37 108 **(6.6%)**	39 060 **(6.6%)**
VIIRS only	107 873 **(16.3%)**	85 598 **(15.9%)**	82 340 **(14.7%)**	85 885 **(14.6%)**
Valid points				
Valid matchup points	110 033 **(16.6%)**	85 437 **(15.8%)**	72 197 **(12.9%)**	82 854 **(14.1%)**
Within CTH Spec	43 525 **(6.6%)**	39 743 **(7.4%)**	31 234 **(5.6%)**	36 778 **(6.2%)**
Within CBH Spec	49 925 **(7.5%)**	41 580 **(7.7%)**	32 568 **(5.8%)**	38 385 **(6.5%)**
Percentage of Valid points that are Within CTH Spec	39.6%	46.5%	43.3%	44.4%
Percentage of Valid points that are Within CBH Spec	45.4%	48.7%	45.1%	46.3%

of the allowed range of 0–20 km MSL [out of range (OOR)], or the pixel was within a "bowtie deletion" line [onboard or on-ground pixel trim (OBPT and OGPT, respectively)]. This nomenclature for fill values follows the JPSS program standards (see, e.g., Seaman et al. 2014). For a detailed discussion of the bowtie effect and bowtie deletion lines in VIIRS data, see Cao et al. (2013b). It should be noted that pixels identified as OBPT or OGPT fill are redundant—because of the bowtie effect, they overlap with a pixel from an adjacent scan. In this work, OBPT/OGPT fill is reported only when all other VIIRS pixels that overlap the *CloudSat* profile also contain fill values and when the OBPT/OGPT pixel is the closest match to *CloudSat* spatially. The geolocation of VIIRS is accurate to within 75 m (Wolfe et al. 2013), and the geolocation of the *CloudSat* CPR is accurate to within 500 m (Tanelli et al. 2008).

For our purposes, a matchup period is defined as the period of time during which *CloudSat* and VIIRS view the same locations on Earth's surface within 15 min of each other. Because VIIRS and *CloudSat* are located at different altitudes on the same orbital plane [i.e., sun-synchronous orbits with a 1330 local time (LT) ascending equator crossing times], these matchup periods occur once every 2–3 days and last for approximately 4.5 h, or about three complete *SNPP* orbits. Table 2 shows the

statistics for each of the matchup periods examined for this study. All matchup periods where *CloudSat* and VIIRS data are available have been analyzed for June 2014, September 2014, January 2015, and April 2015. Figure 2 shows the locations of each of these matchup periods.

For each *CloudSat* profile within a matchup period, the closest nonerror-filled VIIRS CBH retrieval that at least partially overlaps a given *CloudSat* footprint was identified. These *CloudSat* profile–VIIRS pixel pairs comprised the "matchup points." The VIIRS-retrieved CTH and CBH values were compared with those observed by *CloudSat*. Matchup points were excluded from the statistical analysis presented in section 4 (and listed in Table 2) if any of the following conditions were true: (i) either the VIIRS cloud mask or CPR cloud mask failed to detect cloud, (ii) either the VIIRS or *CloudSat* CTH and/or CBH values were less than 1 km AGL or above 20 km MSL, (iii) precipitation was identified in the *CloudSat* profile, or (iv) all VIIRS pixels that at least partially overlapped with the *CloudSat* profile were error filled. Matchup points that were not excluded by this filter comprised the set of "valid" matchup points. Results were stratified by cloud phase and optical thickness as retrieved by VIIRS. The differences between VIIRS- and *CloudSat*-retrieved boundaries (for both CTH and CBH) are referred to as the "error."
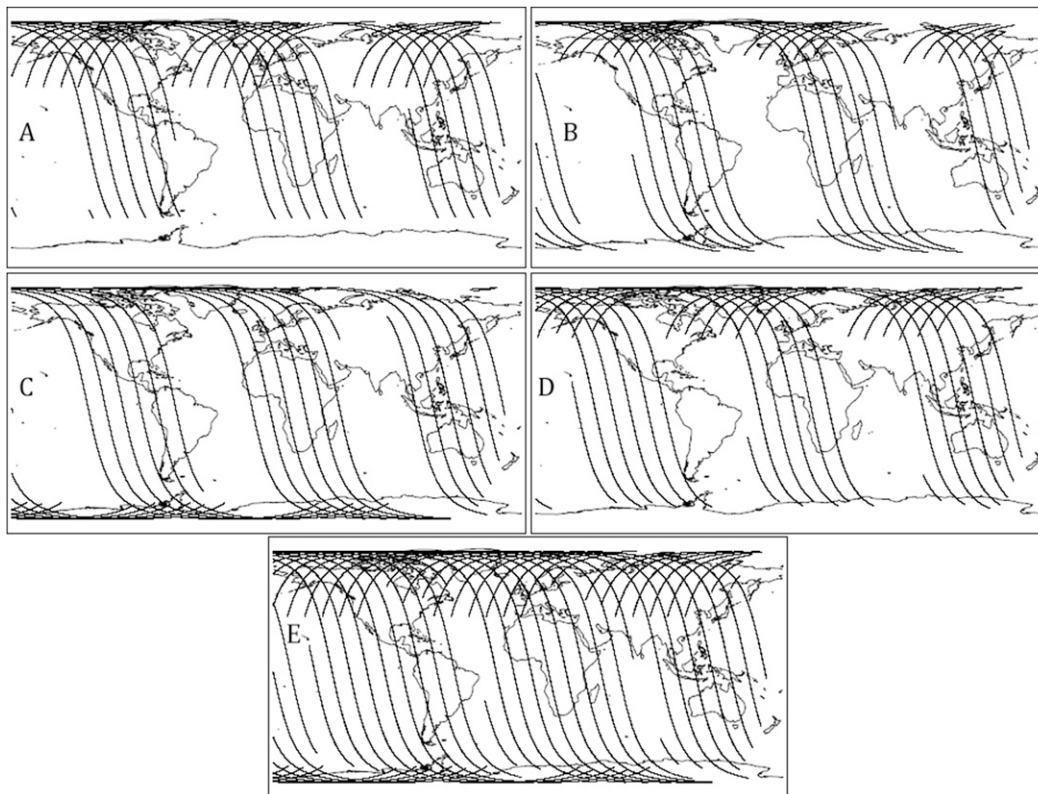
FIG. 2. Locations of the matchup points for (a) June 2014, (b) September 2014, (c) January 2015, (d) April 2015, and (e) the 4 months combined.

The IDPS CTH retrieval is required to meet the following error specifications: the absolute value of the error should be less than 1 km for clouds with $\tau > 1$ (classified as optically thick) and less than 2 km for clouds with $\tau < 1$ (classified as optically thin). As the performance of the CBH retrieval is highly dependent on the accuracy of the CTH retrieval, we further classified matchup points according to this CTH requirement. Matchup points where the CTH error was within the given error specifications are identified as "Within CTH Spec." Furthermore, matchup points where the absolute value of the CBH error is less than 2 km are identified as "Within CBH Spec" (see Table 2). Matchup points where the absolute value of the error was less than 250 m were considered to be "correct," as this is approximately the minimum difference that can be resolved by *CloudSat*.

Removal of VIIRS-retrieved CBH values in the lowest kilometer AGL due to ground clutter in the *CloudSat* CPR inhibits the evaluation of the IDPS CBH product as it relates to low cloud ceiling observations that may be most relevant to aviation interests. However, this and other exclusions discussed above ensure that the comparison between VIIRS and *CloudSat* is

limited to those profiles where the *CloudSat* CBH values are most trustworthy. As the retrieval of CBH from VIIRS is constrained by the distance between the surface and the retrieved CTH, the IDPS CBH will by definition meet the error specifications set by the JPSS program for clouds with CTH less than 2 km AGL. As a result of the matchup criteria presented above, the analysis presented in the next section is weighted toward clouds above the boundary layer, where it is more useful to determine whether the IDPS CBH algorithm meets requirements. An evaluation of the IDPS CBH algorithm using ground-based observations has been performed that focuses on clouds in the lower troposphere (Fitch et al. 2016).

4. Results

Figure 3 shows examples of *CloudSat*–VIIRS matchups for two VIIRS granules. The gray shading indicates the vertical profile of clouds as given by the *CloudSat* cloud mask. The color shaded regions indicate the vertical profile of clouds as given by the VIIRS CTH and CBH retrievals, with colors corresponding to the VIIRS cloud phase classification. The difference in
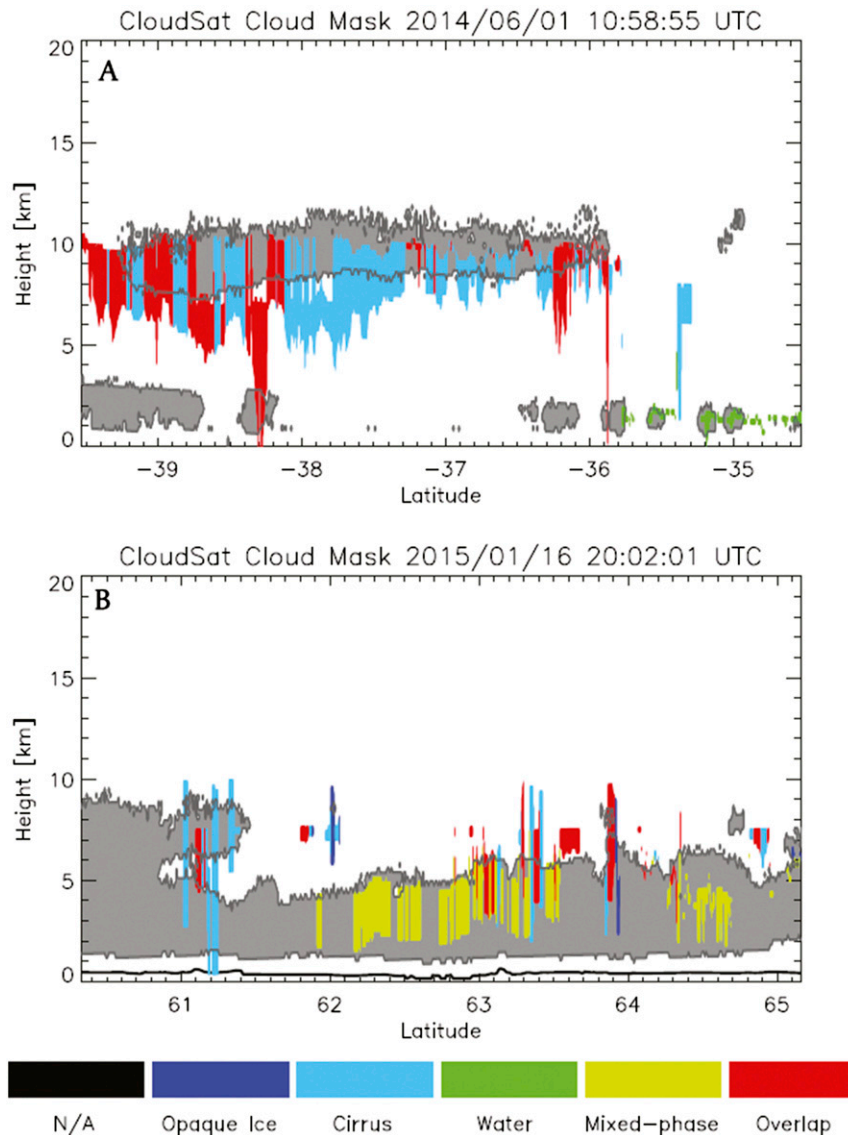
FIG. 3. Examples of the comparison between the *CloudSat* cloud mask (gray shading) and the VIIRS vertical cloud profiles as given by the IDPS CTH and CBH retrievals (colored) for the VIIRS granules at (a) 1058 UTC 1 Jun 2014 and (b) 2002 UTC 16 Jan 2015. Colors correspond to the VIIRS-retrieved cloud phase given by the legend. The thick black line represents land surface elevation. The time given corresponds to the start time of the VIIRS granule that matches the *CloudSat* profile.

height between the top of the color shading and the top of the gray shading represents the CTH error. Likewise, the difference in height between the bottom of the color shading and the bottom of the gray shading for the uppermost cloud layer represents the CBH error. In this work, the *CloudSat*-retrieved value of CTH (or CBH) was subtracted from the VIIRS-retrieved value to determine the error. Thus, a positive error indicates the VIIRS CTH (or CBH) is higher than the *CloudSat* CTH (or CBH). A negative error indicates the *CloudSat*-retrieved value is greater than the VIIRS-retrieved value.

Based on the comparison of the IDPS CBH with the *CloudSat*-derived CBH for these four 1-month periods (a total of 350 521 valid matchup points), statistics of the errors were compiled. The CBH statistics for all valid matchup points and for each cloud phase class, including mean error (bias), median error, standard deviation, root-mean-square error (RMSE), and the correlation coefficient (r^2) are provided (Table 3). Figure 4 shows

TABLE 3. Statistics of VIIRS IDPS CBH retrieval performance as compared to *CloudSat* observations for all valid matchup points included in this work. Note that a negative error means the VIIRS CBH value is less than the *CloudSat* CBH value.

Cloud phase	All clouds	Cirrus	Opaque ice	Mixed phase	Water	Overlap
Matchup points	350 521	113 832	21 240	51 655	67 052	96 742
Bias (km)	−0.7	−1.4	0.8	−0.3	−1.2	−0.3
Median error (km)	−0.3	−1.5	0.8	0.1	0.0	−0.5
Std dev of error (km)	3.6	3.7	3.2	2.7	3.2	4.1
RMSE (km)	3.7	3.9	3.3	2.7	3.4	4.1
r^2 correlation	0.185	0.061	0.037	0.016	0.119	0.004
Percentage of Correct retrievals	1.5%	2.2%	1.0%	1.6%	3.6%	1.7%

the scatterplots of CBH and CTH for all valid matchup points in the dataset. In this figure, colors represent the number of points in each 0.5-km height bin according to a base-10 logarithmic scale. Figure 5 shows the corresponding error histograms, colored according to the VIIRS-retrieved cloud optical thickness, plotted on linear and logarithmic axes. The linear-axis histograms (Fig. 5a) highlight the errors that dominate the "all clouds" error statistics (shown in Table 4), while the logarithmic-axis histograms (Fig. 5b) highlight the distribution of errors found at higher optical depths, which are hidden at the bottom of the scale in Fig. 5a due to the relatively small number of matchup points with large optical depth.

While a sharp peak exists in the overall error histogram near 250 m (black curve in Fig. 5a), the associated scatterplot (Fig. 4a) shows no particular tendency for CBH retrievals to fall along the 1-to-1 line. This peak in the histograms is dominated by the high number of clouds with cloud bases near 1 km MSL. The matchups for low clouds are expected to have the smallest errors,

since CBH errors cannot exceed the distance between the CTH and the surface. Thus, for boundary layer clouds, CBH errors cannot exceed the depth of the boundary layer. In contrast, for upper-tropospheric clouds, the upper constraint on CBH errors is the depth of the troposphere. As may be expected by the considerable spread in the scatterplot in Fig. 4a, the corresponding r^2 are extremely small (Table 3). For all clouds globally and for each cloud phase classification, only a small percentage of the retrievals were found to be correct to within the vertical resolution of the *CloudSat* CPR, and the RMSE and standard deviation values both exceeded the JPSS program specifications. And, as shown in Table 2, less than half of all valid matchup points were found to have errors less than 2 km (Within CBH Spec).

Figure 6 compares the *CloudSat* cloud mask and VIIRS cloud vertical profiles for several examples that highlight known issues with the IDPS CBH retrieval. Figure 6a shows an example where the IWC parameterization produced large CGT errors and an associated CBH at or near the surface for an upper tropospheric
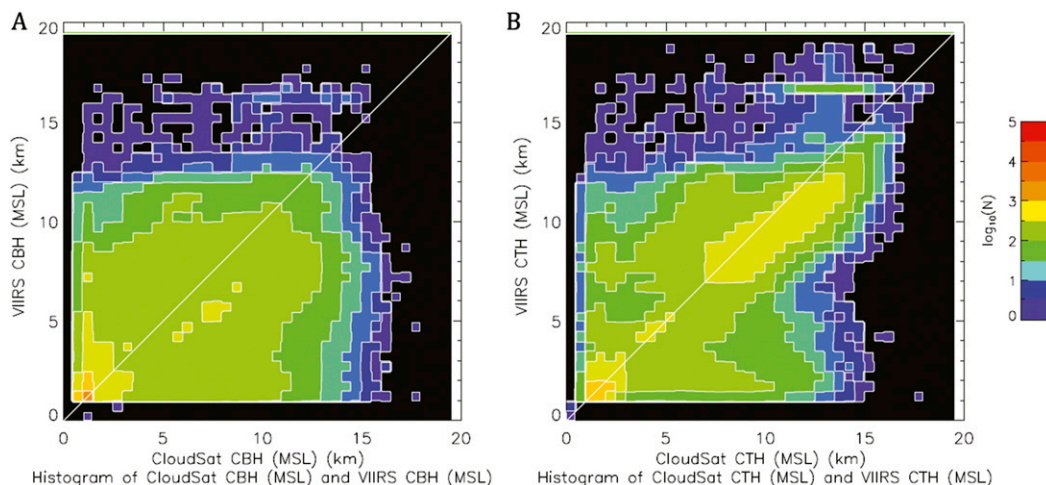

FIG. 4. Two-dimensional histograms (scatterplots) of VIIRS retrievals vs *CloudSat* retrievals for (a) CBH and (b) CTH. In each figure, colors represent the number of points in each 0.5-km height bin according to the logarithmic scaling to the right of (b). The white diagonal lines represent the 1-to-1 line.
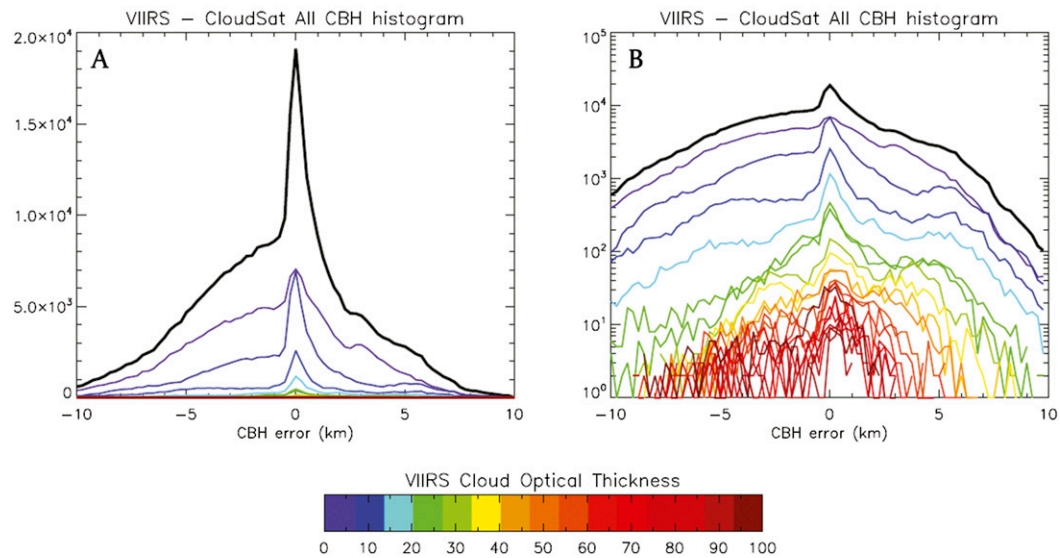
FIG. 5. Histograms of VIIRS vs *CloudSat* CBH errors shown on (a) linear and (b) logarithmic axes. The black curve represents all valid matchup points. Colored curves represent error histograms for clouds with VIIRS-retrieved optical thickness values given by the legend.

cirrus cloud. It should be noted that these large CBH errors have been excluded in the statistics presented in Table 3, as the retrieved CBH falls within the 1-km AGL "exclusion zone," where ground clutter prevents *CloudSat* from validating CBH for these pixels. In Fig. 6b, the CGT values retrieved by the IDPS algorithm are approximately accurate for most of the cirrus cloud profiles in this example. However, the CTH errors are on the order of 2–4 km and this leads to similar errors in CBH. CTH is often underestimated in optically thin cirrus clouds (Heidinger et al. 2010a,b). In Fig. 6c, the VIIRS retrievals fail to detect the upper cloud layer. While the CTH and CBH values appear accurate for the lower layer of clouds, the analysis here focuses on the topmost cloud layer. The failure to detect the upper cloud layer results in CTH and CBH errors of 5–8 km.

Figure 6d shows several issues. Pixels identified as mixed phase have accurate CTH, while the CBH is

overestimated due to significant underestimation of CGT. Pixels not identified as mixed phase in Fig. 6d are found to have an underestimated CBH due to an over-estimated CGT. These errors arise even though the cloud layer is of nearly uniform geometric thickness according to *CloudSat*, suggesting that the thresholds in the cloud phase classification can lead to significant errors in the IDPS CBH retrieval.

Other issues related to cloud phase and type classification discovered during the course of this analysis include pixels identified as opaque ice having a retrieved COT less than 1 (not shown), pixels identified as cirrus and not opaque ice when the retrieved COT was greater than 100 (not shown), and pixels identified as water clouds having a retrieved CTH and/or CBH value above 10 km MSL. Figure 7 shows the two-dimensional histogram (scatterplot) for the subset of valid matchup points classified as water clouds by the VIIRS cloud phase

TABLE 4. Statistics of VIIRS IDPS CBH retrieval performance as compared to *CloudSat* observations for the subset of valid matchup points where the CTH retrieval was Within CTH Spec. Note that a negative error means the VIIRS CBH value is less than the *CloudSat* CBH value.

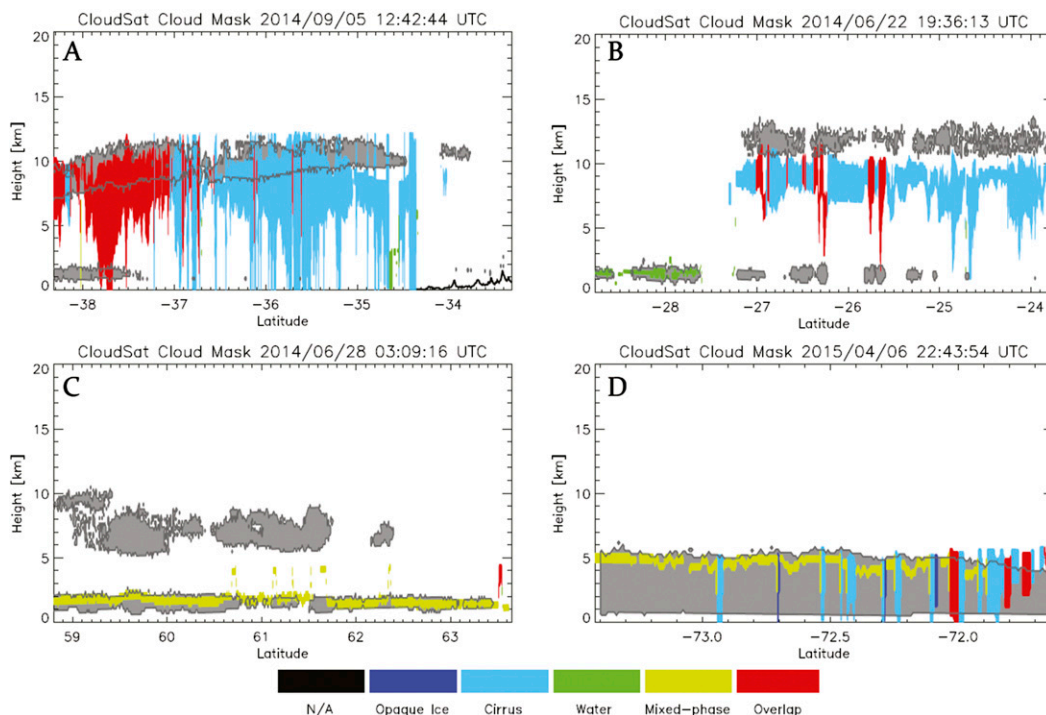| Cloud phase	All clouds	Cirrus	Opaque ice	Mixed phase	Water	Overlap
Matchup points	151 274	50 672	8589	23 599	36 674	31 740
Bias (km)	−0.4	−1.1	−0.1	0.4	0.3	−1.0
Median error (km)	0.0	−0.7	0.1	0.4	0.2	−0.7
Std dev of error (km)	2.3	2.9	2.3	1.3	0.6	2.6
RMSE (km)	2.3	3.0	2.3	1.3	0.7	2.8
r^2 correlation	0.569	0.186	0.222	0.372	0.835	0.219
Percentage of Correct retrievals	19.4%	8.2%	9.1%	23.0%	44.2%	8.6%

FIG. 6. As in Fig. 3, but for VIIRS granules at (a) 1242 UTC 5 Sep 2014, (b) 1936 UTC 22 Jun 2014, (c) 0309 UTC 28 Jun 2014, and (d) 2243 UTC 6 Apr 2015, illustrating various issues with the CBH retrieval as described in the text.

classification. Note the points in the upper-left corner in Fig. 7, where clouds detected above 10 km MSL by VIIRS were classified as water, despite this being physically impossible, due to the homogeneous freezing level occurring below this height. It is possible that these are cases where optically thin cirrus overrode optically thick liquid clouds (not flagged as cloud overlap) and the liquid signal dominated the ice signal in the cloud phase classification. A much higher number of points were found near the lower-right corner of Fig. 7. These are points where *CloudSat* detected an upper-level cloud that either the VIIRS retrievals failed to detect or were optically thin enough that the CTT retrieval placed CTH in the lower troposphere.

Based on Figs. 6a, 6c, and 7, caution must be used when interpreting the statistics presented in Table 3. In many cases, large CBH errors due to the IWC parameterization within the IDPS CBH retrieval were not included in Table 3 because *CloudSat* is not able to validate CBH values < ~1 km AGL. Clouds identified as cirrus should not have a retrieved CBH < 1 km AGL, which is a problem with the IDPS CBH algorithm. At the same time, the Table 3 statistics do include large errors when the VIIRS retrievals and *CloudSat* profiles are in disagreement over whether an upper-tropospheric cloud exists, and these errors are not the fault of the IDPS CBH algorithm. The dataset analyzed here contained 66 988

matchup points that were classified as cirrus, yet had a retrieved CBH less than 1 km AGL and were excluded from Table 3. In contrast, there were 32 122 matchup points where CTH errors exceeded 5 km that were not excluded. This suggests that this analysis is more likely to
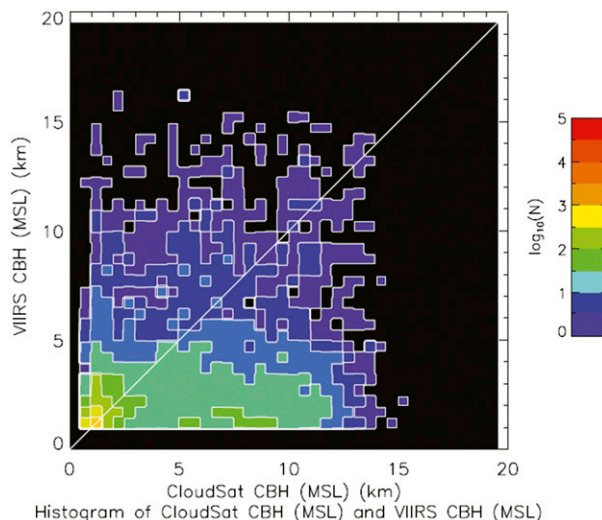

FIG. 7. Two-dimensional histogram (scatterplot) of VIIRS CBH vs *CloudSat* CBH for matchup points classified as water clouds by the VIIRS cloud phase retrieval. Colors and legend are as in Fig. 4.
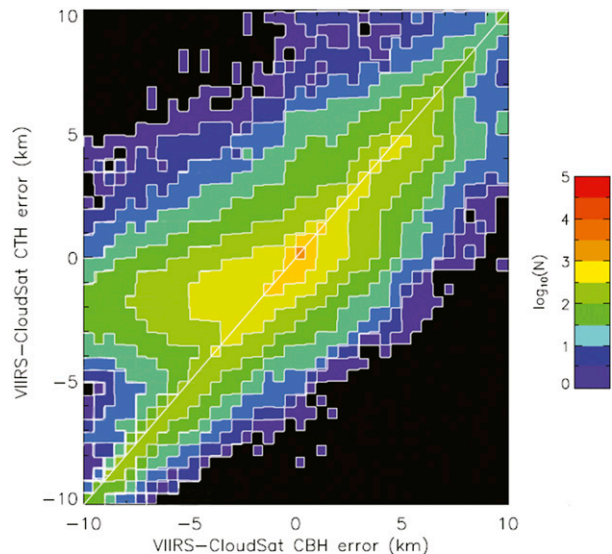
FIG. 8. Two-dimensional histogram (scatterplot) of VIIRS CTH errors vs VIIRS CBH errors for all valid matchup points. Colors and legend are as in Fig. 4.

exclude large errors within the CBH product than to include large errors due to large disagreements in CTH. However, users of the IDPS CBH algorithm should be aware that large CBH errors exist in these situations.

Figure 8 shows the scatterplot of VIIRS CTH errors versus VIIRS CBH errors for all valid matchup points. In each CTH error bin, the mode of the CBH error distribution falls near the 1-to-1 line, indicating that CBH error is highly correlated with CTH error. As expected, it is unlikely for CBH errors to be small when CTH errors are large. Note also that there is significant spread on either side of the 1-to-1 line, particularly when the absolute value of the CTH error is less than ~2 km. This indicates that CTH error alone does not explain the full breadth of CBH errors.

As the CBH retrieval cannot fairly be expected to have small errors when the two satellite instruments disagree on the existence of high clouds or when large CTH errors exist, a second set of statistics was compiled for the Within CTH Spec matchup points. These points are the subset of points where the CTH errors were less than the error specifications defined by the JPSS program and outlined in section 3. The Within CTH Spec dataset eliminates large CTH errors as a source of CBH errors, and it may be considered an evaluation of the CGT retrieval performance, rather than the overall performance of the CBH product. Statistics for the Within CTH Spec matchup points are shown in Table 4. The associated CBH scatterplot (Fig. 9) and error histograms (Fig. 10) are also shown. Even with a high

correlation in CTH between VIIRS and *CloudSat* ($r^2 = 0.970$), the correlation in CBH is only moderate for all clouds ($r^2 = 0.569$) and RMSE values fail to meet the specifications for three of the five cloud phase classes. The tails on the CBH error histogram (Fig. 10) extend out to ±5 km, and in rare cases CBH errors can still exceed 10 km—even when the CTH is within the error specifications. It is possible that *CloudSat* is observing the base of the topmost layer of a multilayered cloud system, but the VIIRS retrievals consider the multi-layered cloud as one integrated deep cloud. Another possibility is that the temperature-dependent IWC parameterization, which, as discussed in section 2, is known to overestimate CGT for cold clouds, is responsible for the large errors. The negative bias and larger tail on the negative side of the error distribution indicate that the IDPS CBH retrieval is more likely to underestimate CBH relative to *CloudSat*—meaning the CGT retrieval has a tendency to overestimate the actual cloud geometric thickness. This is shown more clearly in Fig. 11, which shows the two-dimensional histogram (scatterplot) of CBH error versus COT for the Within CTH Spec matchup points. At nearly all optical depths, more matchup points were found to have negative error than a positive error.

While large CBH errors may still exist with the Within CTH Spec subset of matchup points, there is a dramatic improvement in the IDPS CBH performance for water clouds (cf. Tables 3 and 4). This improvement arises primarily because we have eliminated from consideration cases where VIIRS and *CloudSat* disagree on the presence of an upper-tropospheric
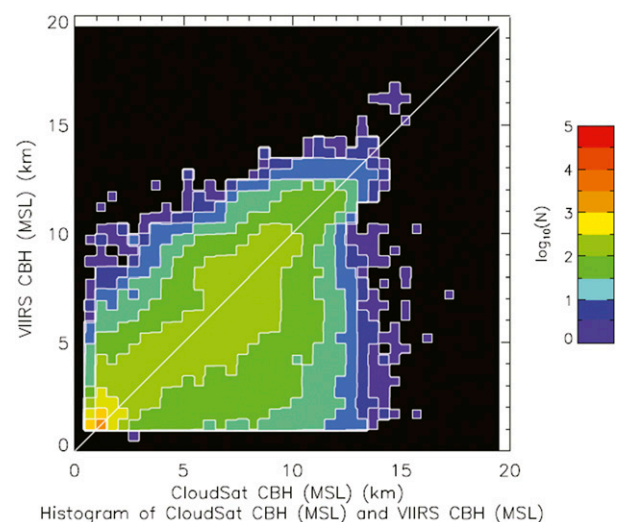

FIG. 9. Two-dimensional histogram (scatterplot) of VIIRS CBH vs *CloudSat* CBH for all matchup points where CTH is Within CTH Spec. Colors and legend are as in Fig. 4.
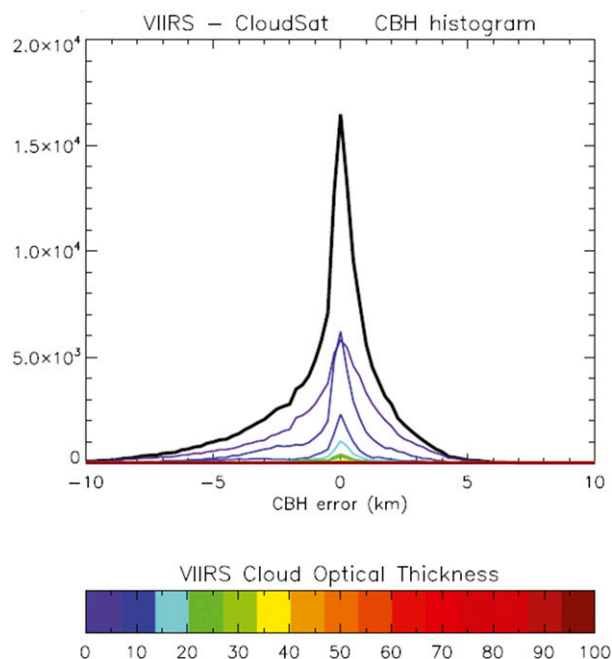
FIG. 10. As in Fig. 5a, but for the subset of matchup points where the CTH retrieval is Within CTH Spec.

cloud layer. Improvements are found for all other cloud types as well, suggesting that the CBH retrieval offers some skill when the CTH retrievals are reasonably accurate.

To better gauge the skill of the CGT component of the CBH retrieval, results from the Within CTH Spec dataset were compared against a broad-brush assumption on CGT that is expected to have no skill. In this experiment, all clouds were assumed to have a CGT of 2 km, indiscriminate of cloud type, properties, or level in the atmosphere; that is, CBH = CTH − 2 km for all clouds. Results of this experiment for the Within CTH Spec matchup points are shown in Table 5, and corresponding histograms of the CBH errors are shown in Fig. 12. Values highlighted in bold in Table 5 represent an improvement over the operational IDPS CBH algorithm shown in Table 4. Note the differing number of valid matchup points for each cloud phase classification (cf. Tables 4 and 5) as the static 2-km CGT allows for varying matchup points to fall within or outside of the 1-km AGL ground clutter exclusion zone. In particular, more clouds classified as water were excluded as the 2-km CGT yields a CBH value less than 1 km AGL. In contrast, more cirrus, opaque ice, and "overlap" points were included, as the IWC parameterization no longer results in the retrieval of upper-tropospheric cloud CBH values below 1 km AGL.

While care must be taken in the analysis of the statistics shown in Table 5, particularly in comparison with

Table 4, it is clear that assuming a constant CGT value of 2 km improves the VIIRS CBH retrieval for both cirrus and overlap clouds. Even for opaque ice clouds, the VIIRS cloud phase classification that is the most likely to exceed 2 km in geometric thickness, the results are mixed as to whether assuming a constant CGT of 2 km is an improvement over the current IDPS algorithm. The constant CGT assumption clearly degrades the performance of the CBH retrieval for water clouds when compared to the IDPS retrieval, however, as these clouds were often less than 1 km thick. The performance for mixed-phase clouds is similar between Tables 4 and 5. For all clouds on the whole, it may be stated that the IDPS CBH retrieval does not clearly outperform a simple assumption of a constant 2-km cloud geometric thickness.

5. Conclusions

The retrieval of Hutchison (2002) and Hutchison et al. (2006), which relates retrievals of cloud optical thickness (COT) and effective particle size (EPS) to cloud geometric thickness (CGT) and, ultimately, cloud-base height (CBH), became the first operational global retrieval of CBH from passive visible and infrared satellite sensors upon the launch of the *SNPP* satellite and the VIIRS instrument. The JPSS program has implemented this algorithm through the IDPS, which was responsible
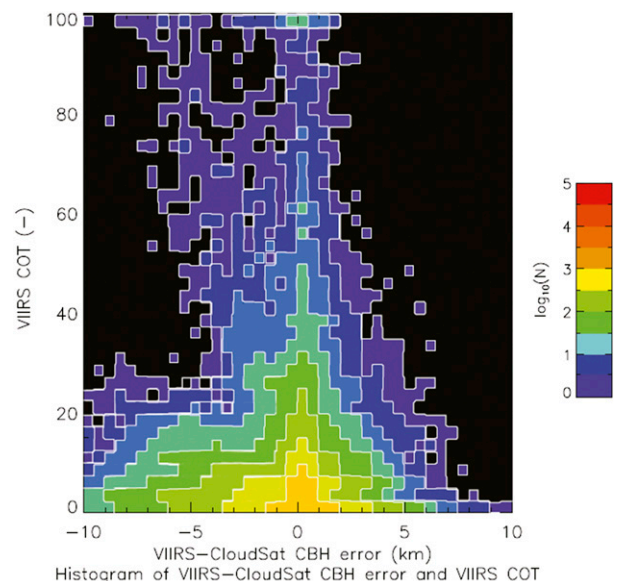

FIG. 11. Two-dimensional histogram (scatterplot) of CBH error vs VIIRS COT for the subset of matchup points where the CTH retrieval is Within CTH Spec. Colors represent the number of points in each 0.5-km error/2.5 optical thickness bin according to the logarithmic scaling indicated on the right.

TABLE 5. Statistics of VIIRS CBH retrieval performance as compared to *CloudSat* observations for the subset of valid matchup points where the CTH retrieval was Within CTH Spec and all clouds were assumed to have a CGT of 2 km. Bold values indicate improvement over the IDPS CBH retrieval results shown in Table 4. Note that a negative error means the VIIRS CBH value is less than the *CloudSat* CBH value.

Cloud Phase	All clouds	Cirrus	Opaque ice	Mixed phase	Water	Overlap
Matchup points	154 205	69 361	16 230	22 298	4292	42 024
Bias (km)	**0.1**	**−0.3**	1.0	**−0.2**	−0.8	**0.6**
Median error (km)	−0.2	**−0.5**	0.9	**−0.2**	−0.8	**0.2**
Std dev of error (km)	**1.9**	**1.7**	**2.2**	**1.2**	1.2	**2.2**
RMSE (km)	**1.9**	**1.7**	2.4	**1.2**	1.5	**2.3**
r^2 correlation	**0.634**	**0.598**	**0.273**	0.367	0.791	**0.417**
Percentage of Correct retrievals	11.3%	**9.8%**	8.2%	20.5%	15.9%	**9.4%**

for the operational production and distribution of all JPSS products following the launch of *SNPP*.

In this work, the IDPS CBH retrieval product was compared against spatially and temporally matched CBH observations from *CloudSat* operational data products. The matches take care to account for parallax displacement, filter out precipitation-contaminated CPR observations, and avoid the surface clutter region. While these filters significantly limit the scope of the validation, they provide the subset of data where the validations are most trustworthy. For these data where *CloudSat* could best be regarded as "truth," significant errors in the IDPS CBH retrieval are found. More than half of all CBH retrievals had errors exceeding the 2-km error requirement set by the JPSS program. The RMSE for all clouds was found to be 3.7 km. Linear (r^2) correlations between the VIIRS-based and *CloudSat* CBH values were less than 0.2 for all cloud types. Errors were also found to exceed ±10 km on occasion, which represents nearly the entire depth of the troposphere. A comparison between the IDPS CBH algorithm and ground-based observations of CBH for lower-troposphere clouds also showed retrieval errors exceeding the 2-km accuracy requirement with linear (r^2) correlations no greater than 0.38 (Fitch et al. 2016).

The most common causes of large CBH errors were found to be 1) the temperature-dependent IWC, resulting in a large overestimate of CGT and hence a corresponding underestimate of CBH for cold ice-phase clouds; and 2) VIIRS and *CloudSat* observations in disagreement over whether the uppermost cloud layer was located in the upper or lower troposphere. Large CBH errors were also associated with large CTH errors, even when both instruments detected the same cloud layer (e.g., Fig. 6b). It was found that only 40%–45% of all valid matchup points had an IDPS CTH retrieval that was "Within CTH Spec" when compared against *CloudSat* observations of CTH. However, the CALIOP lidar on board the *CALIPSO* satellite is better suited to validate the IDPS CTH retrieval product (Baker 2012).

Errors in COT, EPS, and CTT can result in the misclassification of cloud type and cloud phase used by the IDPS CBH algorithm, leading to errors in the retrieved CBH.

To better test the retrieval of cloud geometric thickness—the primary component of the CBH retrieval—a subset of the matchup points was analyzed for cases where CTH errors were within the JPSS program error specifications. This Within CTH Spec dataset eliminates large CTH disagreement as a source of CBH errors. An analysis of the Within CTH Spec dataset showed that the IDPS CBH retrieval had modest skill when the CTH retrieval had reasonable agreement with *CloudSat*. However, it was shown that the skill of the IDPS retrieval is tempered by the fact that it performs no better
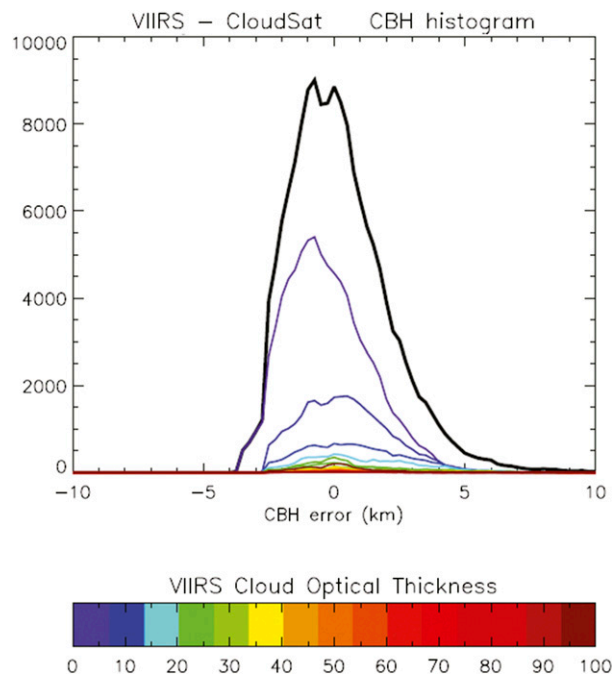

FIG. 12. As in Fig. 10, except all clouds were assumed to be 2 km thick in the VIIRS CBH retrieval.

overall than a retrieval that assumes a constant cloud geometric thickness of 2 km.

From a practical user perspective, the fact that large errors in CBH exist is more important than the exact cause of the large errors. However, improvement of the CBH algorithm requires the ability to distinguish errors resulting from within the CBH algorithm and those errors that originate in upstream retrievals. The analysis of all valid matchup points demonstrates the overall performance of the CBH product, with no attempt made to exclude upstream errors. The analysis of the Within CTH Spec dataset excludes large CTH errors as a source of CBH error. However, this analysis is not capable of distinguishing between CBH errors caused by COT and EPS errors, misclassification of cloud type and phase, or the predefined LWC values. It was shown that large CBH errors may still exist even when CTH errors were small, suggesting that errors from these other sources are significant.

The IDPS CBH retrieval algorithm has several readily apparent shortcomings. It is dependent on a number of upstream retrievals—a failure in any of which will prevent the retrieval of CBH. Errors in these upstream retrievals lead directly to errors in CBH. As discussed in Heidinger et al. (2010a,b), the IDPS CTH retrieval is based on IR emission and as a result the CTH that is retrieved represents the effective level of emission, which typically occurs at some depth within the cloud layer (depending on the cloud optical properties) and is thus biased lower in the atmosphere than the CTH determined by active sensors (i.e., CALIOP on board *CALIPSO*). The CBH retrieval examined here, which is dependent on an accurate CTH as input, inherits this same bias. Values of LWC are assumed to be constant across the globe, varying only by cloud type classification. Aircraft observations of stratocumulus clouds show that LWC may vary by up to two orders of magnitude, depending on region (e.g., land vs ocean) and other factors (Miles et al. 2000), and it is reasonable to assume the same is true for other cloud types. The IWC parameterization produces extremely small values of IWC for cloud-top temperatures less than ∼220 K when the optical thickness is small and produces errors in cloud geometric thickness of an order of magnitude or more (Baker 2011). The relationship between LWP and cloud optical thickness assumes a constant droplet effective radius throughout the entire cloud layer (Stephens 1994), which is not likely to be true for most clouds. Also, the IDPS algorithm has no way to account for clouds that contain both liquid droplets and ice particles. The current algorithm assumes all mixed-phase clouds are ice clouds for the purpose of estimating CGT. Mixed-phase clouds comprise a significant fraction of clouds globally and many of these clouds contain liquid water at cloud top (see, e.g., Noh et al. 2011 and references therein). Deep convective clouds often contain ice on top with liquid water at and near cloud base, and this is also not accounted for in the CBH retrieval algorithm.

Given the known limitations of the IDPS CBH retrieval and its performance shortfalls, as shown in this work, it would be worthwhile to explore possible improvements or alternative approaches to the current operational algorithm. Statistics of IWC retrieved directly from the *CloudSat* CPR (Austin et al. 2009) or CALIOP lidar (Heymsfield et al. 2005) could be used to improve the IWC parameterization used in the CBH algorithm by better quantifying the likely IWC values for thin cirrus clouds. Improved quality controls on the operational algorithm could include performing cloud type uniformity tests (driving the selection of LWC/IWC, and potential strong discontinuities at artificial cloud type interfaces), capping CGT to physically reasonable values, and improving the performance of upstream parameters feeding into the algorithm. Additional quality controls could be introduced as well. For example, in the case of deep convective clouds where the COT signal is saturated and CBH would be difficult and highly uncertain to retrieve, it may be better to enlist numerical weather prediction model airmass property information to determine the lifted (or convective) condensation level and use this value as a proxy for the expected location of cloud base. Zhu et al. (2014) developed an algorithm to retrieve convective cloud-base temperature from *SNPP* VIIRS observations that could be used to derive cloud-base height. It may also be possible to relate observed CGT to various cloud properties statistically. These ideas are being actively pursued at this time. A companion paper (Noh et al. 2017) discusses one such alternative approach for retrieving CBH from VIIRS and other similar passive visible and IR satellite observations.

and Atmospheric Administration (NOAA), JPSS Program Office, or U.S. government position, policy, or decision.

REFERENCES

Austin, R. T., A. J. Heymsfield, and G. L. Stephens, 2009: Retrieval of ice cloud microphysical parameters using the CloudSat millimeter-wave radar and temperature. *J. Geophys. Res.*, **114**, D00A23, doi:10.1029/2008JD010049.

Baker, M. B., 1997: Cloud microphysics and climate. *Science*, **276**, 1072–1078, doi:10.1126/science.276.5315.1072.

Baker, N., 2011: Joint Polar Satellite System (JPSS) VIIRS cloud base height algorithm theoretical basis document (ATBD). JPSS Ground Project Code 474-00045, NASA GSFC, 35 pp. [Available online at http://www.star.nesdis.noaa.gov/jpss/documents/ATBD/D0001-M01-S01-015_JPSS_ATBD_VIIRS-Cloud-Base-Height.pdf.]

——, 2012: Joint Polar Satellite System (JPSS) VIIRS cloud top algorithm theoretical basis document (ATBD). Revision A, JPSS Ground Project Code 474-00041, NASA-GSFC, 73 pp. [Available online at http://www.star.nesdis.noaa.gov/jpss/documents/ATBD/D0001-M01-S01-012_JPSS_ATBD_VIIRS-Cloud-Top_A.pdf.]

——, 2013: Joint Polar Satellite System (JPSS) operational algorithm description (OAD) document for VIIRS perform parallax correction (PPC) intermediate product (IP) software. Revision B, JPSS Ground Project Code 474-00088, NASA GSFC, 28 pp. [Available online at http://npp.gsfc.nasa.gov/sciencedocs/2015-06/474-00088_OAD-VIIRS-PPC-IP_B.pdf.]

——, 2014: Joint Polar Satellite System (JPSS) VIIRS cloud mask (VCM) algorithm theoretical basis document (ATBD). Revision E, JPSS Ground Project Code 474-00033, NASA GSFC, 101 pp. [Available online at http://www.star.nesdis.noaa.gov/jpss/documents/ATBD/D0001-M01-S01-011_JPSS_ATBD_VIIRS-Cloud-Mask_E.pdf.]

Bankert, R. L., M. Hadjimichael, A. P. Kuciauskas, W. T. Thompson, and K. Richardson, 2004: Remote cloud ceiling assessment using data mining methods. *J. Appl. Meteor.*, **43**, 1929–1946, doi:10.1175/JAM2177.1.

Bendix, J., B. Thies, J. Cermak, and T. Nauss, 2005: Ground fog detection from space based on MODIS daytime data—A feasibility study. *Wea. Forecasting*, **20**, 989–1005, doi:10.1175/WAF886.1.

Calvert, C. G., M. J. Pavolonis, S. Hubbard, C. M. Gravelle, and S. S. Lindstrom, 2016: The GOES-R/JPSS approach for identifying hazardous low clouds: Overview and operational impacts. *12th Annual Symp. on New Generation Operational Environmental Satellite Systems*, New Orleans, LA, Amer. Meteor. Soc., 8.4. [Available online at https://ams.confex.com/ams/96Annual/webprogram/Paper290493.html.]

Cao, C., J. Xiong, S. Blonski, Q. Liu, S. Uprety, X. Shao, Y. Bai, and F. Weng, 2013a: Suomi NPP VIIRS sensor data record verification, validation and long-term performance monitoring. *J. Geophys. Res. Atmos.*, **118**, 11 664–11 678, doi:10.1002/2013JD020418.

——, and Coauthors, 2013b: Visible Infrared Imaging Radiometer Suite (VIIRS) sensor data record (SDR) user's guide. Version 1.2, NOAA Tech. Rep. NESDIS 142A, 46 pp. [Available online at http://www.star.nesdis.noaa.gov/jpss/documents/UserGuides/VIIRS_SDR_Users_Guide.pdf.].

Eberhard, W. L., 1986: Cloud signals from lidar and rotating beam ceilometer compared with pilot ceiling. *J. Atmos. Oceanic Technol.*, **3**, 499–512, doi:10.1175/1520-0426(1986)003<0499:CSFLAR>2.0.CO;2.

Ellrod, G. P., 2002: Estimation of low cloud base height at night from satellite infrared and surface temperature data. *Natl. Wea. Dig.*, **26** (12), 39–44.

Fitch, K. E., K. D. Hutchison, K. S. Bartlett, R. S. Wacker, and K. C. Gross, 2016: Assessing VIIRS cloud base height products with data collected at the Department of Energy Atmospheric Radiation Measurement sites. *Int. J. Remote Sens.*, **37**, 2604–2620, doi:10.1080/01431161.2016.1182665.

Forsythe, J. F., T. H. Vonder Haar, and D. Reinke, 2000: Cloud-base height estimates using a combination of meteorological satellite imagery and surface reports. *J. Appl. Meteor.*, **39**, 2336–2347, doi:10.1175/1520-0450(2000)039<2336:CBHEUA>2.0.CO;2.

Fuchs, B. R., and Coauthors, 2015: Environmental controls on storm intensity and charge structure in multiple regions of the continental United States. *J. Geophys. Res. Atmos.*, **120**, 6575–6596, doi:10.1002/2015JD023271.

Goldberg, M. D., H. Kilcoyne, H. Cikanek, and A. Metha, 2013: Joint Polar Satellite System: The United States next generation civilian polar-orbiting environmental satellite system. *J. Geophys. Res. Atmos.*, **118**, 13 463–13 475, doi:10.1002/2013JD020389.

Gultepe, I., and Coauthors, 2009: The Fog Remote Sensing and Modeling Field Project. *Bull. Amer. Meteor. Soc.*, **90**, 341–359, doi:10.1175/2008BAMS2354.1.

Haynes, J. M., T. S. L'Ecuyer, G. L. Stephens, S. D. Miller, C. Mitrescu, N. B. Wood, and S. Tanelli, 2009: Rainfall retrieval over the ocean with spaceborne W-band radar. *J. Geophys. Res.*, **114**, D00A22, doi:10.1029/2008JD009973.

Heidinger, A. K., M. J. Pavolonis, R. E. Holz, B. A. Baum, and S. Berthier, 2010a: Using CALIPSO to explore the sensitivity to cirrus height in the infrared observations from NPOESS/VIIRS and GOES-R/ABI. *J. Geophys. Res.*, **115**, D00H20, doi:10.1029/2009JD012152.

——, ——, ——, ——, and ——, 2010b: Correction to "Using CALIPSO to explore the sensitivity to cirrus height in the infrared observations from NPOESS/VIIRS and GOES-R/ABI." *J. Geophys. Res.*, **115**, D12299, doi:10.1029/2010JD014461.

Herzegh, P., G. Wiener, R. Bateman, J. Cowie, and J. Black, 2015: Data fusion enables better recognition of ceiling and visibility hazards in aviation. *Bull. Amer. Meteor. Soc.*, **96**, 526–532, doi:10.1175/BAMS-D-13-00111.1.

Heymsfield, A. J., D. Winker, and G.-J. van Zadelhoff, 2005: Extinction-ice water content-effective radius algorithms for CALIPSO. *Geophys. Res. Lett.*, **32**, L10807, doi:10.1029/2005GL022742.

Hillger, D., and Coauthors, 2013: First-light imagery from Suomi NPP VIIRS. *Bull. Amer. Meteor. Soc.*, **94**, 1019–1029, doi:10.1175/BAMS-D-12-00097.1.

Hutchison, K., 2002: The retrieval of cloud base heights from MODIS and three-dimensional cloud fields from NASA's EOS Aqua mission. *Int. J. Remote Sens.*, **23**, 5249–5265, doi:10.1080/01431160110117391.

——, E. Wong, and C. Ou, 2006: Cloud base heights retrieved during night-time conditions with MODIS data. *Int. J. Remote Sens.*, **27**, 2847–2862, doi:10.1080/01431160500296800.

Inoue, M., A. D. Fraser, N. Adams, S. Carpenter, and H. E. Phillips, 2015: An assessment of numerical weather prediction–derived low-cloud-base height forecasts. *Wea. Forecasting*, **30**, 486–497, doi:10.1175/WAF-D-14-00052.1.

Johnson, D. B., 1980: The influence of cloud-base temperature and pressure on droplet concentration. *J. Atmos. Sci.*, **37**, 2079–2085, doi:10.1175/1520-0469(1980)037<2079:TIOCBT>2.0.CO;2.

Kokhanovsky, A. A., and V. V. Rozanov, 2005: Cloud bottom altitude determination from a satellite. *IEEE Trans. Geosci. Remote Sens. Lett.*, **2**, 280–283, doi:10.1109/LGRS.2005.846837.

Lawson, R. P., and B. A. Baker, 2006: Improvement in determination of ice water content from two-dimensional particle imagery. Part II: Applications to collected data. *J. Appl. Meteor. Climatol.*, **45**, 1291–1303, doi:10.1175/JAM2399.1.

Leyton, S. M., and J. M. Fritsch, 2004: The impact of high-frequency surface weather observations on short-term probabilistic forecasts of ceiling and visibility. *J. Appl. Meteor.*, **43**, 145–156, doi:10.1175/1520-0450(2004)043<0145:TIOHSW>2.0.CO;2.

Liou, K.-N., 1992: *Radiation and Cloud Processes in the Atmosphere: Theory, Observation and Modeling. Oxford Monogr. Geol. Geophys.*, Vol. 20, Oxford University Press, 504 pp.

Mace, G. G., and Q. Zhang, 2014: The CloudSat radar–lidar geometrical profile product (RL-GeoProf): Updates, improvements, and selected results. *J. Geophys. Res. Atmos.*, **119**, 9441–9462, doi:10.1002/2013JD021374.

Marchand, R., G. G. Mace, T. Ackerman, and G. Stephens, 2008: Hydrometeor detection using *CloudSat*—An Earth-orbiting 94-GHz cloud radar. *J. Atmos. Oceanic Technol.*, **25**, 519–533, doi:10.1175/2007JTECHA1006.1.

Miles, N. L., J. Verlinde, and E. E. Clothiaux, 2000: Cloud droplet size distributions in low-level stratiform clouds. *J. Atmos. Sci.*, **57**, 295–311, doi:10.1175/1520-0469(2000)057<0295:CDSDIL>2.0.CO;2.

Miller, S. D., and Coauthors, 2014: Estimating three-dimensional cloud structure from statistically blended active and passive sensor observations. *J. Appl. Meteor. Climatol.*, **53**, 437–455, doi:10.1175/JAMC-D-13-070.1.

Minnis, P., and Coauthors, 1997: Cloud optical property retrieval (subsystem 4.3). CERES Algorithm Theoretical Basis Doc. 4.3, Release 2.2, 60 pp. [Available online at http://ceres.larc.nasa.gov/atbd.php.]

Nayak, M., M. Witkowski, D. Vane, T. Livermore, and M. Rokey, 2012: CloudSat anomaly recovery and operational lessons learned. *Proc. 12th Int. Conf. on Space Operations (Space Ops 2012)*, Stockholm, Sweden, CNES, 1295798. [Available online at http://www.spaceops2012.org/proceedings/documents/id1295798-Paper-001.pdf.]

Noh, Y.-J., C. J. Seaman, T. H. Vonder Haar, D. R. Hudak, and P. Rodriguez, 2011: Comparisons and analyses of aircraft and satellite observations for wintertime mixed-phase clouds. *J. Geophys. Res.*, **116**, D18207, doi:10.1029/2010JD015420.

——, and Coauthors, 2017: Cloud-base height estimation from VIIRS. Part II: A statistical algorithm based on A-Train satellite data. *J. Atmos. Oceanic.*, **34**, 585–598, doi:10.1175/JTECH-D-16-0110.1.

Ou, S. C., K. N. Liou, and T. R. Caudill, 1998: Remote sounding of multilayer cirrus cloud systems using AVHRR data collected during FIRE-II-IFO. *J. Appl. Meteor.*, **37**, 241–254, doi:10.1175/1520-0450-37.3.241.

——, Y. Takano, K. N. Liou, G. J. Higgins, A. George, and R. Slonaker, 2003: Remote sensing of cirrus cloud optical thickness and effective particle size for the National Polar-orbiting Operational Environmental Satellite System Visible/Infrared Imager Radiometer Suite: Sensitivity to instrument noise and uncertainties in environmental parameters. *Appl. Opt.*, **42**, 7202–7214, doi:10.1364/AO.42.007202.

Pandey, P. C., E. G. Njoku, and J. W. Waters, 1983: Inference of cloud temperature and thickness by microwave radiometry from space. *J. Climate Appl. Meteor.*, **22**, 1894–1898, doi:10.1175/1520-0450(1983)022<1894:IOCTAT>2.0.CO;2.

Reinke, D. L., and T. H. Vonder Haar, 2011: Probability of cloud-free-line-of-sight derived from CloudSat and CALIPSO cloud observations. *2011 EUMETSAT Meteorological Satellite Conf.*, Oslo, Norway, EUMETSAT. [Available online at http://www.eumetsat.int/website/home/News/ConferencesandEvents/DAT_2039705.html.]

Schmit, T. J., M. M. Gunshor, W. P. Menzel, J. J. Gurka, J. Li, and A. S. Bachmeier, 2005: Introducing the next-generation Advanced Baseline Imager on GOES-R. *Bull. Amer. Meteor. Soc.*, **86**, 1079–1096, doi:10.1175/BAMS-86-8-1079.

Seaman, C., D. Hillger, T. Kopp, R. Williams, S. Miller, and D. Lindsey, 2014: Visible Infrared Imaging Radiometer Suite (VIIRS) imagery environmental data record (EDR) user's guide. Version 1.1, NOAA Tech. Rep. NESDIS 147, 30 pp. [Available online at http://www.star.nesdis.noaa.gov/jpss/documents/UserGuides/VIIRS_Imagery_EDR_Users_Guide.pdf.]

Slingo, A., and J. M. Slingo, 1988: The response of a general circulation model to cloud longwave forcing. I: Introduction and initial experiments. *Quart. J. Roy. Meteor. Soc.*, **114**, 1027–1062, doi:10.1002/qj.49711448209.

Stephens, G. L., 1994: *Remote Sensing of the Lower Atmosphere.* Oxford University Press, 540 pp.

——, and Coauthors, 2002: The CloudSat mission and the A-Train: A new dimension of space-based observations of clouds and precipitation. *Bull. Amer. Meteor. Soc.*, **83**, 1771–1790, doi:10.1175/BAMS-83-12-1771.

——, and Coauthors, 2008: CloudSat mission: Performance and early science after the first year of operation. *J. Geophys. Res.*, **113**, D00A18, doi:10.1029/2008JD009982.

Sun, X. J., H. R. Li, H. W. Barker, R. W. Zhang, Y. B. Zhou, and L. Liu, 2016: Satellite-based estimation of cloud-base heights using constrained spectral radiance matching. *Quart. J. Roy. Meteor. Soc.*, **142**, 224–232, doi:10.1002/qj.2647.

Tanelli, S., S. L. Durden, E. Im, K. S. Pak, D. G. Reinke, P. Partain, J. M. Haynes, and R. T. Marchand, 2008: CloudSat's Cloud Profiling Radar after two years in orbit: Performance, calibration, and processing. *IEEE Trans. Geosci. Remote Sens.*, **46**, 3560–3573, doi:10.1109/TGRS.2008.2002030.

Walther, A., A. K. Heidinger, and S. D. Miller, 2013: The expected performance of cloud optical and microphysical properties derived from Suomi NPP VIIRS day/night band lunar reflectance. *J. Geophys. Res. Atmos.*, **118**, 13 230–13 240, doi:10.1002/2013JD020478.

Wilheit, T. T., and K. D. Hutchison, 1997: Retrieval of cloud base heights from passive microwave data constrained by infrared based cloud information. *Int. J. Remote Sens.*, **18**, 3263–3278, doi:10.1080/014311697217071.

Winker, D. M., M. A. Vaughan, A. H. Omar, Y. Hu, K. A. Powell, Z. Liu, W. H. Hunt, and S. A. Young, 2009: Overview of the CALIPSO mission and CALIOP data processing algorithms. *J. Atmos. Oceanic Technol.*, **26**, 2310–2323, doi:10.1175/2009JTECHA1281.1.

Wolfe, R. E., G. Q. Lin, M. Nishihama, K. P. Tewari, J. C. Tilton, and A. R. Isaacman, 2013: Suomi NPP VIIRS prelaunch and on-orbit geometric calibration and characterization. *J. Geophys. Res. Atmos.*, **118**, 11508–11521, doi:10.1002/jgrd.50873.

Zhu, Y., D. Rosenfeld, X. Yu, G. Liu, J. Dai, and X. Xu, 2014: Satellite retrieval of convective cloud base temperature based on the NPP/VIIRS Imager. *Geophys. Res. Lett.*, **41**, 1308–1313, doi:10.1002/2013GL058970.